Melt Duration on Glaciers: Environmental Controls Examined with Orbiting Radar

J. GRAHAM COGLEY[1], M.A. ECCLESTONE[1], AND D.T. ANDERSEN[2]

ABSTRACT

Direct, in-situ measurements of glacier mass balance are expensive. Remote sensing would be an attractive alternative if remotely-observable quantities could be interpreted in terms of mass gain or loss. A system developed recently for the analysis of Radarsat browse images is used here to explore temporal and environmental controls of melting on glaciers on Axel Heiberg Island, Nunavut, Canada. The browse images have an effective spatial resolution of 2 km, are georeferenced to single-pixel accuracy, and number about 200 over the two study years, 1998 and 1999. Surface melting in the accumulation zone is readily recognized by the strong contrast in brightness between bright cold firn, which exhibits a microwave signal dominated by volume scattering from ice lenses and pipes, and dark wet firn, the signal from which is muted by either absorption or near-specular reflection at the surface. In the ablation zone, radar images, apart from showing the brief spring period of snowmelt, contain little information about the intensity or even the fact of melting. We show, however, that in the accumulation zone there is a definite dependence of brightness on temperature: at temperatures above freezing, the hotter it is the darker does the appearance of the glacier become. This is most naturally (and encouragingly) interpreted as a relation between brightness and melting rate. Analysis of same-day image pairs shows that, as expected, terrain slope and aspect influence radar brightness strongly and must therefore be allowed for in future modelling of the hydrology of ablation on glaciers.

Key words: Glaciers, ablation, synthetic aperture radar, Axel Heiberg Island.

INTRODUCTION

In glaciology and glacial hydrology there are powerful incentives to explore remote sensing as a way of increasing information. The quest for a means of estimating glacier mass balance and its components from space has been pursued for a quarter of a century (Østrem 1975), and although useful ideas and insight have resulted (e.g. Braithwaite 1984; Demuth and Pietroniro 1999) there are still no remotely-obtained estimates of mass balance. Optical sensors are limited by darkness and especially by cloud cover, and discriminating between snow and bare ice at these wavelengths remains a scientific challenge. Passive microwave sensors such as SSM/I have low spatial resolution, appropriate for the study of ice sheets (Zwally and Fiegles 1994; Abdalati and Steffen 1997) but not of smaller ice bodies such as valley glaciers. Active synthetic aperture radar (SAR) sensors such as ERS-1,2 and Radarsat suffer none of these limitations, although the cost of acquisition can be a limiting factor and even with modern computing power the handling of large numbers of images calls for substantial resources.

[1]Department of Geography, Trent University, Peterborough, Ontario, Canada K9J 7B8
[2]Department of Geography, McGill University, Montreal, Quebec, Canada H3A 2T5

Browse images, offered as image selection tools by organizations such as the Canada Centre for Remote Sensing, are free even of these practical problems. Their marginal cost to the organization is small, they cost nothing to the user, and they make negligible demands on computer mass storage. For Radarsat imagery the spatial resolution, about 2 km, is of course worse than the 100 m of the full ScanSAR images which the browse images represent. Assuming generously that the 8-bit quantization of the browse images implies a halving of the radiometric resolution, a browse image contains about 800 times less information than its original image and is thus a very sparse sample. But there is no reason to believe that the browse image offers a biassed view of the scene illuminated by the radar. Browse images may therefore have intrinsic merit as study media, but of course they may also be seen as exploratory tools for future operational systems relying on full images.

This work is a reconnaissance in which, using substantial numbers of browse images, we explore the temporal dimension of radar remote sensing which is opened up by sacrificing spatial resolution. The aim is to identify promising ways of tackling the practical problem of estimating meltwater production rates on glaciers. We shall focus on: distinguishing between frozen and melting states of the glacier surface; tracking the seasonal evolution of melting conditions; refining the description of relationships between radar brightness and terrain elevation, and radar brightness and temperature; and exploring the contribution of topography to the microwave signal from glacier surfaces.

Image Processing

Cogley (2001) developed and described a system for processing and analysis of browse images obtained from the search engine at the web site of the Canada Centre for Remote Sensing (URL: http://ceonet.cgdi.gc.ca/cs/en/ index.html). A much-improved search engine became available after images were collected for this study (URL: http://ceocat.ccrs.nrcan.gc.ca/ quicklook/quicklook.html). Sources of guidance during development of the image analysis system included Curlander and McDonough (1991), Olmsted (1993) and Seeber (1993).

Table 1. Metadata accompanying Radarsat browse images.

Information	Remarks
Date and time	Time obtained from image file name
Orbit number	
Ascending/descending orbit flag	
Image position within satellite scan	Scan over study region may be split into more than one image
Ground receiving station	
Radar beam and mode	Radarsat is able to emit several beams of different extents; all images studied here are ScanSAR Wide mode images built from four beams at once
Angle of incidence at image centre	Not used
Image centre coordinates	Geographical; not used
Image corner coordinates	Geographical
Image width and height	Typically 256x256 pixels; supplied by JPEG decompression algorithm

Briefly, the browse images are 256x256-pixel, 8-bit JPEG representations of full ScanSAR scenes which are typically about 540 km on a side. Effective resolution is therefore about 2 km. The system georeferences each image by relying in part on limited accompanying metadata (Table 1) and in part on correlation of the image with a library of mask chips. The image information is first transferred geometrically to a map with 2-km resolution in the Universal Transverse Mercator projection. Nearest-neighbour resampling ensures that the mean and variance of image brightness are preserved in the map, although there is necessarily an ambiguity of the order of 1 km in the horizontal position of the mapped brightness. The result is a draft map of radar brightness with positional

accuracy of a few kilometres or better. The mask chips are small samples from a land-sea mask (see below) and are used for fine adjustment of the draft map. The map-to-mask correlation algorithm depends on there being a marked contrast of image brightness between land and sea. This requirement is met in the great majority of images, and it is reasonable to claim sub-pixel locational accuracy for the final product.

A radiometric terrain correction is applied to the mapped brightness. For each target (estimated ground position of an image pixel), we construct a vector pointing to the satellite. For each map cell we construct from a digital elevation model (DEM; see below) the mean outward normal of the surface. The angle between these two unit vectors is an estimate of the local angle of incidence i_L of the radar beam. Each brightness s is multiplied by the factor $\sin i_L / \sin i_H$, where i_H is the angle of incidence on a horizontal surface at sea level at the location of the map cell. This has the nominal result (Raney 1998) of transforming s to the brightness of an equivalent horizontal surface. In fact, although the correction reduces modestly but noticeably the contrast between slopes of different orientation and steepness, the corrected signal still contains substantial terrain-related noise. This is due in part to the neglect of volume scattering and in part to the fact that the correction is purely radiometric; no geometric terrain corrections are applied.

Topographic Information

Glacier outlines were digitized from 1:250 000 scale topographic maps and used to construct a glacier mask. The maps are based on aerial photography at 1:56 000 scale flown in 1958 and 1959. Although glacier margins are known to have changed between the late 1950s and the 1990s we can be confident, for example from the measurements of Cogley et al. (1996a) and more informal comparisons of recent and older imagery, that the changes are negligible at the scale and resolution of this study. The mask consists of 8-bit fractions (255ths) of glacier cover in cells of size 1x1 km. On the basis of these fractions and of land-cover fractions obtained similarly from digitized shorelines, 2x2 km map cells are allotted to the categories sea, land and ice by summation and the use of appropriate cutoffs.

A digital elevation model of the study region was constructed from the GLOBE database (Hastings and others 1999). At the latitude of Axel Heiberg Island this 30" (30-arc-second) database has zonal and meridional resolutions of 160 m and 925 m respectively, yielding about 20 samples for each 2x2 km cell in the maps used here. The DEM elevation is the median of these sample elevations.

There is some question, however, about the accuracy of the GLOBE elevation data, which derive from 1:1 000 000 scale maps based on Corona satellite imagery of the early 1960s with typical scales of 1:300 000 to 1:400 000; the contour interval is 305 m (1000 feet). Through the courtesy of M. Sharp of the University of Alberta we were able to compare the GLOBE elevations with Canadian Digital Elevation Data (CDED; Centre for Topographic Information 2000) over much of our study region. The CDED database derives from the same 1:250 000 maps and 1:56 000 photography as our land and glacier masks. It has meridional resolution of 3" and zonal resolution of 6" (12" north of 80°N), or 92 m by 32 to 64 m. The contour interval on the parent maps is 152 m (500 feet; 61 m, or 200 feet, on a few of the maps). We generated a 2x2 km DEM from CDED using the same sorting and median-selection rule as for the GLOBE DEM.

Table 2 summarizes the comparison between GLOBE and CDED. No account was taken of whether points were or were not glacierized, although the number of glacierized GLOBE points is included in the table for information. At higher elevations GLOBE appears to be systematically 10-20 m higher than CDED. Further comparisons of the two data sources with high-resolution DEMs of parts of central Axel Heiberg Island, based on large-scale mapping with in-situ ground control, are in progress. For now, we adopt the rms difference over the entire elevation range, 98 m or ~100 m, as a measure of the uncertainty in a typical 2x2 km elevation estimate obtained from GLOBE. The topographic comparisons reported below have coarse vertical resolution so as to reduce the impact of this uncertainty, and of the ambiguity of pixel position, on interpretation. It should also be noted that both GLOBE and CDED, although they present information at a scale comparable to the footprint of the radar, 100 m, are strongly smoothed representations of the topography because they are derived by interpolation between contours with low vertical resolution.

Table 2. Comparison of CDED and GLOBE DEMs of Axel Heiberg Island.

Elevation band (m)	Mean difference (m)	Rms difference (m)	N	N_g
0- 200	-4.6± 1.4	75.7	3092	116
200- 400	7.9± 1.9	88.5	2086	307
400- 600	11.2± 3.1	125.3	1626	463
600- 800	9.2± 3.3	110.5	1147	789
800- 1000	10.1± 3.8	106.4	762	1107
1000- 1200	20.0± 4.4	114.9	670	632
1200- 1400	24.6± 4.2	101.0	539	601
1400- 1600	12.5± 5.6	85.7	234	288
1600- 1800	3.2± 7.5	76.8	107	85
1800- 2000	26.2±10.1	57.0	26	41
2000- 2200	103.8±21.0	110.0	4	0
0- 2200	6.8± 1.0	98.1	10293	4429

Individual differences are CDED sample medians minus GLOBE sample medians. Rms: root mean square. N: number of 2x2 km CDED cells with corresponding GLOBE elevations. N_g: number of glacierized GLOBE cells.

GLACIERIZATION OF AXEL HEIBERG ISLAND

Axel Heiberg Island, Nunavut, Canada has an area of 37 200 km^2, of which 11 700 km^2 is glacierized (Figure 1). It extends between latitudes 78.1° N and 81.4° N, and has a mountainous north-south axis which rises to elevations over 2 000 m. We selected it for study because of long familiarity and because it has been thoroughly studied in the past. Ommanney (1969) presented a complete glacier inventory of the island. Annual measurements of mass balance have been made in the centre of the island on White Glacier (Cogley et al. 1996b) and Baby Glacier (Adams et al. 1998) since 1959-1960. Axel Heiberg Island is well covered by Radarsat imagery because it is at high latitude (and so the satellite orbit allows for a short revisit interval) and because of demand from the Canadian Ice Service for aids to marine navigation.

ANALYSIS

Expectations

Spatial and seasonal variations in the radar appearance of glaciers are now well understood in outline. As summarized by Cogley (2001), and earlier by Hall et al. (2000) among others, several facies are recognizable in the image of the glacier. (In radar glaciology the definition of "facies" is generally extended to incorporate distinctive variations with seasonal time, and to try to accommodate observable radar zonation within the classical system of glacier facies described by, for example, Paterson 1994.)

Microwave photons incident upon cold, deep snow and firn are highly likely to be backscattered towards the radar if there are objects in the snowpack with dimensions of the order of the wavelength of the radiation. For Radarsat this wavelength is 57 mm, and the most plausible candidate backscatterers are therefore ice lenses and pipes formed by the percolation and refreezing of meltwater. In the absence of such objects, as in the dry snow zones of the ice sheets (Fahnestock et al. 1993), backscattering from snow grains is weak and the glacier appears moderately dark. This high-elevation facies is not seen on Axel Heiberg Island. In the percolation zone, however, the ice lenses are expected to return a strong signal and the glacier will appear bright. The appearance should change markedly when meltwater appears at the surface, for now the first medium encountered by the photons, liquid water, is an efficient specular reflector and hides the volume-scattering subsurface; the glacier surface will appear dark. In the ablation zone the microwave signature of glacier ice should be dominated by surface scattering and should be intermediate in brightness between dry snow and

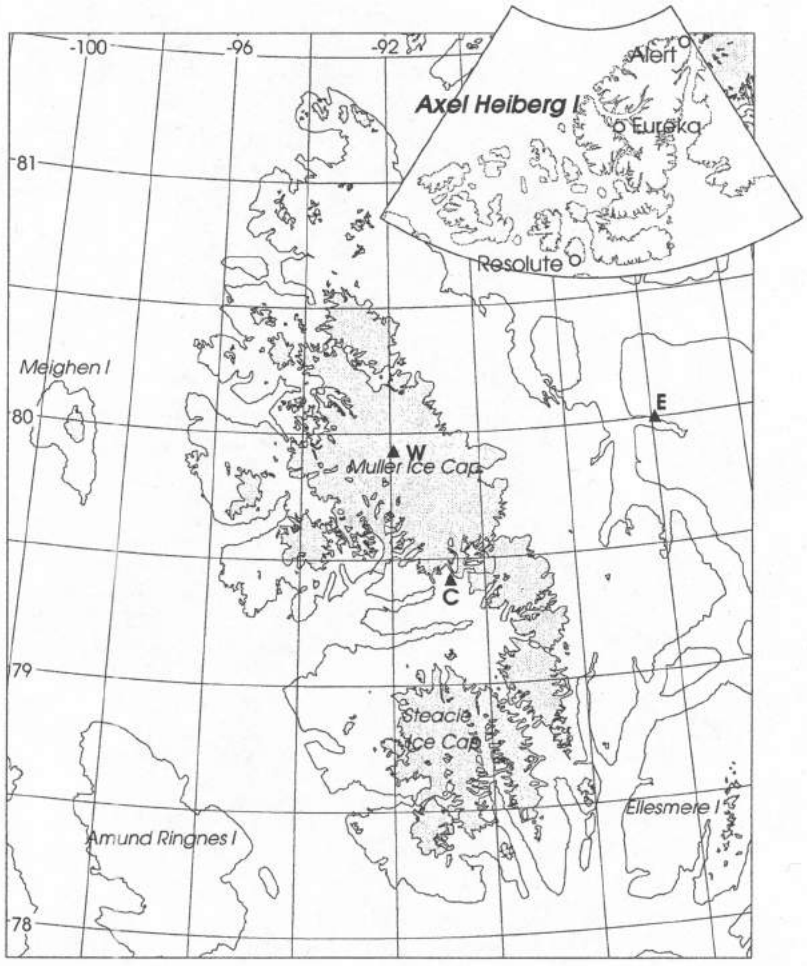

Figure 1. Axel Heiberg Island, showing extent of glacierization and places mentioned in the text. UTM projection, zone 15. C: Colour Lake, which is 3 km southwest of the terminus of Thompson Glacier. E: Eureka. W: White Crown Mountain, 2120 m above sea level.

wet snow. The thin winter snow cover should be transparent to the radar, and surface roughness at scales greater than the wavelength of the incident radiation should affect the received signal noticeably.

In Figure 2 a pair of radar maps is shown to illustrate and confirm the expected contrast between cold and warm conditions. In the November image (Figure 2a) the glacier accumulation zones stand out as very bright, and outlet glaciers such as Thompson Glacier (northeast of Colour Lake; cf. Figure 1) can be seen as dark indentations. Where the ice margin is comparatively regular it is possible to recognize a gradational darkening outwards, but the ice margin itself is difficult to distinguish because the ice is coincidentally similar in tone to the proglacial terrain. In the July image (Figure 2b) almost the entire glacier cover of Axel Heiberg Island is dark, but brighter tones are found on the highest parts of Müller Ice Cap at and southeast of White Crown Mountain. Again an outward gradation of brightness is recognizable, but now the peripheral ice is brighter than the interior.

Seasonal Evolution of Melting

Figure 3 illustrates the seasonal variation of glacier brightness for two calendar years over the study region of Figure 2. The nominal ends of the two balance years, on 1 September, are marked by vertical lines. Roughly, the melt season near to sea level is expected to end around this date, having begun about three months earlier.

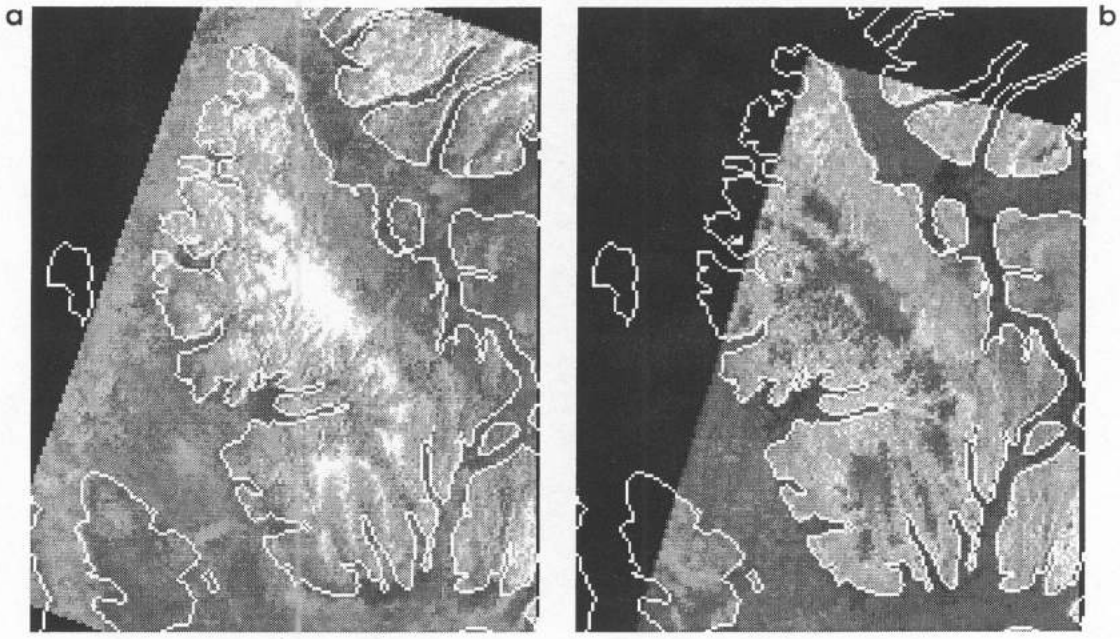

Figure 2. Radar brightness maps of the Axel Heiberg Island region. Pixels represent map cells of size 2x2 km. a: 11 November 1998. b: 26 July 1998. Black bands at the eastern edges of these maps are artefacts of the georeferencing algorithm, which translates the resampled image to maximize its correlation with the land mask.

Several features can be distinguished in Figure 3. 1) There is a long winter during which, at any given time, brightness increases from moderate values near sea level to high values at the highest elevations. 2) A "dark-surface signal" depresses brightness to low values at all elevations during the nominal melt season. By virtue of feature 1, the contrast between winter and melt season increases with elevation; at the lowest elevations its existence may be debatable. 3) The depression of brightness begins, and then becomes most marked, diachronously. The onset and maximum development of the dark-surface signal are up to a month later at higher elevations than near to sea level. 4) The dark-surface signal is considerably more short-lived at the highest elevations, but it is also short-lived at the lowest elevations.

We interpret these features as conforming broadly to the expectations set out above. In winter the percolation zone is bright and the ablation zone is moderately bright. The dark-surface signal represents snowmelt, its duration being short at low elevation because there is little snow and at high elevation because the melt season itself is short. Once spring snowmelt is over, the ablation zone in effect resumes its wintertime appearance.

The accumulated winter snow at low elevations is a thin, dry veneer overlying glacier ice. Although it may contain layers of depth hoar, in which grain size is much coarser than in the bulk of the snowpack, it lacks larger scatterers such as the ice lenses which form in deeper firn when meltwater percolates to depth and refreezes. It should therefore be transparent to the radar. Evidently, however, it is sufficiently thick on average to behave as does the snow surface at higher elevations when melting begins. Until it is dissipated by complete melting, the thin veneer of wetted snow endows the surface with the radiative attributes of liquid water. Once the veneer has disappeared, the surface resumes the appearance proper to glacier ice, for which wet and dry states seem to be indistinguishable. But this may be an oversimplified explanation. Bernier et al. (1999) found that it was possible to estimate snow mass covering boreal terrain in Quebec from radar imagery. They explained the success of their algorithm in terms of the influence of the snow on the temperature and hence the dielectric properties of the underlying soil. An analogous explanation of the phenomena seen in Figure 3 deserves further investigation.

The threshold shown in Figure 3 as a horizontal line is intended only as a plausible guide to interpretation. Clearly, if Figure 3 is to evolve towards quantitative estimation of the duration and

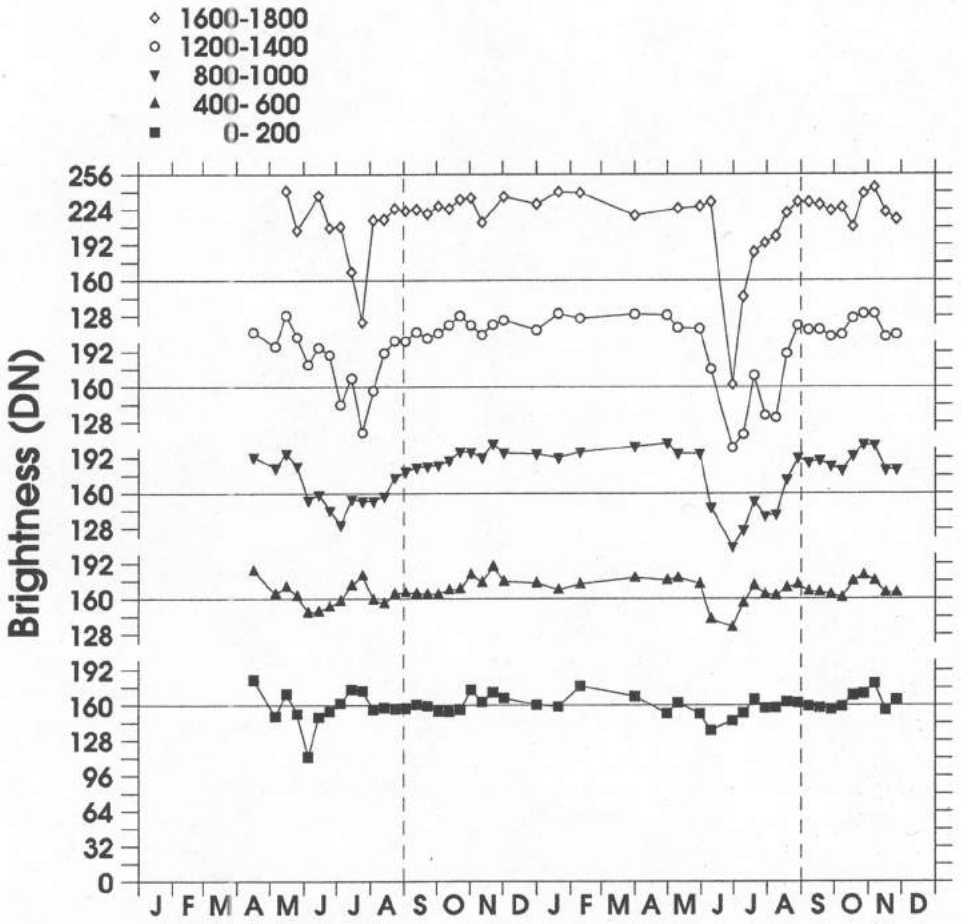

Figure 3. Radar brightness of glacierized map cells as a function of time for selected 200-m elevation bands, 1998-1999. Symbols represent averages over all images within 10-day intervals, with from 0 to 13 images per interval. Most images cover only part of the study region, so the number of samples within each elevation band is somewhat less than the number of glacierized map cells within the band (Table 2). The horizontal line at s=160 represents an arbitrarily chosen threshold brightness which is believed to mark approximately the division between wet snow and dry snow surfaces.

intensity of melting, it will be necessary to model not only the hydrological evolution of the snowpack and its radiometric expression, but also the non-hydrological factors which contribute noise to the time series. These factors consume about half of the dynamic range of the 8-bit digital numbers.

Temperature Dependence of the Microwave Signal

To find out more about the temperature dependence of the microwave signal, we used half-hourly measurements of air temperature made with an automatic weather station at Colour Lake. Colour Lake (Figure 1) is 180 m above sea level at 79.42°N, 90.74°W, 2.5 km from the ice margin in central Axel Heiberg Island. Figure 4 shows the course of temperature variation over the two study years.

Figure 5 shows radar brightness as a function of pixel elevation and adjusted Colour-Lake temperature. All glacierized pixels within the study region were deemed eligible for inclusion. The relationship between surface and free-tropospheric lapse rates in mountainous high-latitude regions is complicated by the persistent near-surface temperature inversion and by our ignorance about how the thickness of the inversion layer varies with surface elevation. We assumed the surface rate to be equal to the atmospheric rate Γ; that is, $T(z) = T_{CL} + \Gamma (z\text{-}z_{CL})$. We use twice-daily upper-air data from Eureka, 120 km from Colour Lake, to estimate the lapse rate at the time of each image. To estimate the rate for each observed atmospheric temperature profile, we first resample, by linear interpolation,

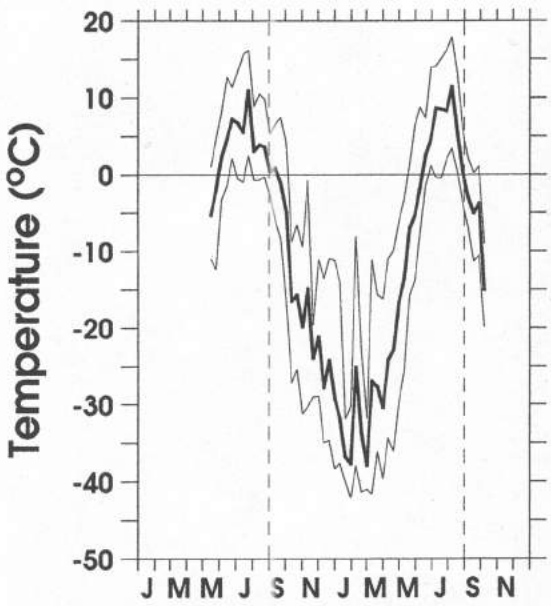

Figure 4. Temperature at Colour Lake, 1998-1999. Thick line: 10-day mean temperature based on half-hourly readings by the automatic weather station. Thin lines: 10-day minimum and maximum half-hourly temperatures.

to a regular 100-m interval in z. Then we locate all runs below $z = 10$ km of consecutive lapse rates more negative than a threshold rate of -3.5 K m^{-1}; select the longest such run; and compute the rate of temperature change over its thickness. Although this scheme is crude, in practice it yields a robust and convincing estimate. If one of the bracketing profiles is too distant in time, the other is used for Γ, while if both are too distant a monthly average is substituted. Otherwise Γ for the Radarsat image is interpolated linearly in time between the two bracketing lapse rates.

The brightness of glacier surfaces at low elevations is independent of temperature. Below 400 m the radar signal appears to convey no information on temperature, and presumably therefore none on temperature-related quantities. Beginning perhaps as low as 400-600 m, but certainly by 800-1000 m, a dependence on temperature emerges and grows increasingly marked as elevation increases. At temperatures well below freezing the glacier surface is bright, with a possible very modest decrease in brightness with temperature. Above -10°C to -5°C, brightness decreases with temperature, and the decrease continues to the highest observed temperatures; the two highest elevation bands depart from this rule, perhaps because sample sizes are small. The variability of brightness tends to be greater at temperatures near and slightly below freezing than at colder or warmer temperatures.

Stiles and Ulaby (1980) showed that liquid water content exerts a strong control on the backscattering coefficient, which decreases with snow wetness. This is the most plausible explanation of the patterns seen in Figure 5: the warmer it is, the wetter will the near-surface snow be and the more completely will its radiative signature obscure the volume-scattering signature of the deeper firn. We should expect, however, that once a snowpack is fully ripe its near-surface wetness will not increase much beyond "field capacity". Once gravity is the dominant force on the liquid water, the water will drain with relative freedom where it is not topographically impeded (e.g. U.S. Army Corps of Engineers 1956). In the coordinate space of Figure 5, this would be represented by a flattening of the curve $s(T)$ at higher T, which is observed only above 1200-1400 m. The most obvious explanation for an increase of snow wetness with temperature is that wetness is proportional to the melting rate, that is, to ablation. Thus it is encouraging from a practical standpoint that brightness remains inversely proportional to temperature even above the freezing point.

It is not clear why the temperature dependence of brightness should be observable to such low elevations. Mass-balance measurements (Cogley et al. 1996b; Haeberli et al. 1999) show that the annual equilibrium line has been above 1000 m in central Axel Heiberg Island throughout the 1990s, except that in 1995-1996 it was as low as 760 m. Thus, below 800 m, the surfaces imaged in 1998 and 1999 were undoubtedly exposed glacier ice rather than residual firn from previous years.

The absence at the lowest elevations of any signal directly related to temperature is unfortunate. Most glaciers on Axel Heiberg Island gain mass at low accumulation rates over extensive high-altitude snowfields, and lose mass at high melting rates on very restricted low-altitude tongues. Not only are the tongues difficult to sample at low spatial resolution, but Figure 5 suggests that we might not be much better off even if this were not so. Microwave estimates of whole-glacier ablation may thus have to be based on downward extrapolation of observations in the accumulation zone.

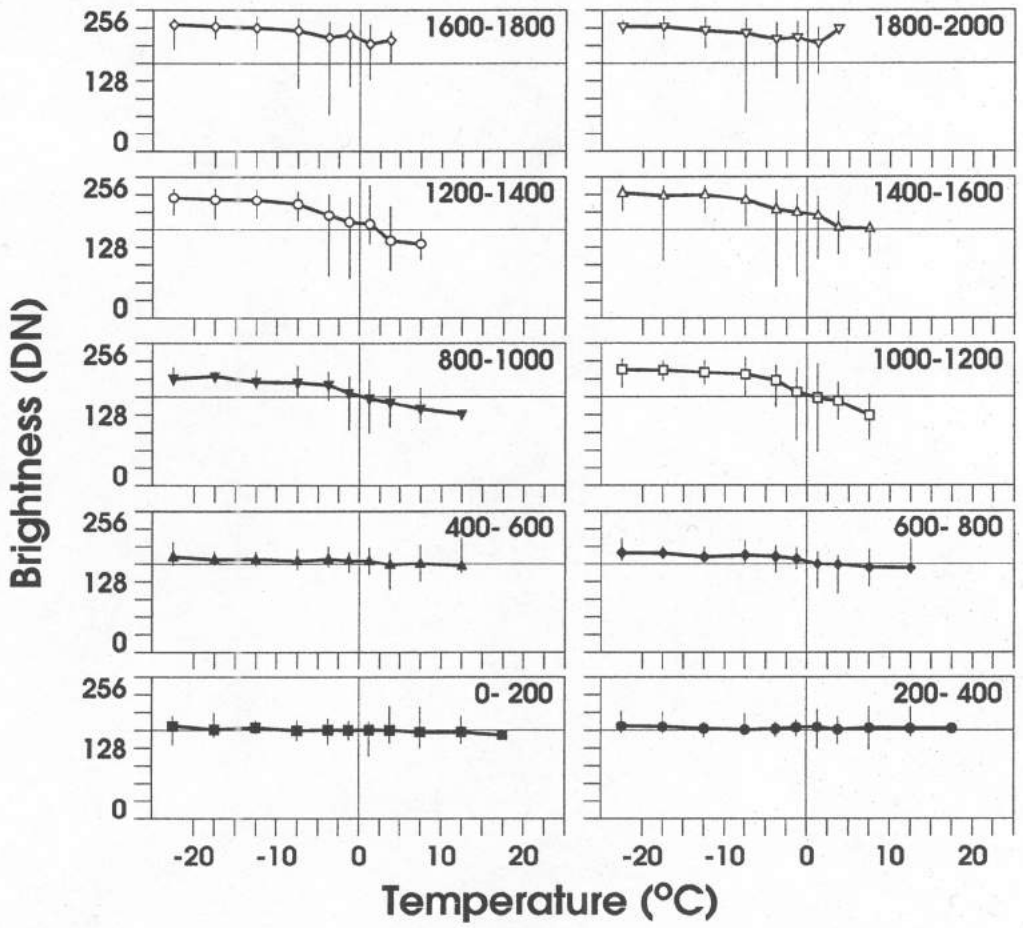

Figure 5. Radar brightness of glacierized map cells as a function of temperature and elevation. Cells were allotted to 200-m elevation bands according to their GLOBE elevations. At the time of each browse image the temperature at Colour Lake was estimated by linear interpolation between half-hourly readings, and was then adjusted to the elevation of each cell by calculating a lapse rate as described in the text. Within each temperature-elevation bin, symbols show the average and vertical lines the observed range of image-average brightnesses.

The variability of brightness near to the freezing point is the combined effect of uncertainty in the assumed lapse rate and real physical variation in the state of the glacier surface. The crudeness of the temperature estimates means that some cold, bright pixels and some warm, dark pixels are assigned to the wrong temperature intervals. Better estimates of temperature as a function of elevation would sharpen the focus of Figure 5.

Dependence of Signal on Viewing Geometry

The time series analyzed above consist of essentially random mixtures of images obtained on ascending and descending satellite overpasses. Radarsat is a polar orbiter in a dawn-dusk orbit, staying close to the terminator so as to maximize solar power receipts. There are two reasons for considering this attribute of the orbit.

First, it means that on descending passes the radar views Axel Heiberg Island at local apparent times of 06-08h while on ascending passes the local time on the glaciers is about 15-17h, and we should expect diurnal variations of the surface to be irregularly represented in the time sequence of images. Second, on ascending passes the radar pulse arrives at the surface from the southwest or west, while on descending passes it arrives from the east or southeast. This means that the local angle of incidence of the radar beam will vary, perhaps significantly or perhaps not, between ascending and

Table 3. Brightness variations with terrain slope and aspect.

Aspect		Slope (deg)						
		<1	1-2	2-3	3-5	5-7	>7	All
Differences:								
Flat		-4.9						
345-	15		-0.3	-2.6	1.8	0.8	1.6	-0.1
15-	45		-15.3	-9.1	-9.0	3.1	-5.8	-10.5
45-	75		-14.4	-12.1	-13.4	-3.6	-2.1	-12.4
75-	105		-10.0	-12.9	-4.5	-2.0	-4.1	-8.1
105-	135		-8.8	-4.2	0.2	12.9	14.6	-1.0
135-	165		-7.6	-3.7	5.9	9.6	4.5	0.3
165-	195		1.0	7.0	0.5	4.3	-2.3	2.6
195-	225		3.4	1.7	6.0	-9.3	-9.7	2.4
225-	255		7.6	7.3	6.9	2.1	-40.0	5.9
255-	285		3.8	3.9	9.4	-0.3	2.0	5.3
285-	315		9.0	3.5	2.9	5.5	-3.8	4.5
315-	345		4.6	2.2	7.7	4.7	13.2	5.2
All			-3.7	-1.8	1.2	2.1	-2.2	
Counts:								
Flat		8342						
345-	15		1032	547	655	172	89	2495
15-	45		1268	1057	923	224	23	3495
45-	75		1892	1154	1213	451	97	4807
75-	105		1211	1496	1954	386	42	5089
105-	135		710	872	1215	375	117	3289
135-	165		667	649	896	286	37	2535
165-	195		673	616	836	332	73	2530
195-	225		1080	897	1047	290	69	3383
225-	255		1081	1960	1898	615	84	5638
255-	285		1173	1162	1610	544	85	4574
285-	315		675	947	1013	270	109	3014
315-	345		673	570	694	323	70	2330
All			12135	11927	13954	4268	895	

Differences: averages over glacierized map cells as a function of slope and aspect (from the CDED DEM) of s_{asc} - s_{des} from analyses of 20 same-day pairs. "Flat" means that terrain slope is less than 1°. Counts: number of samples. The grand-mean azimuths of the sensor are 109.2° for descending (morning) passes and 234.1° for ascending (afternoon) passes. Single-image means are within a few degrees of the grand means, and the range of single-cell azimuths over each image is about 20°.

descending passes if the surface has any topographic or other directional grain. The grain may be at any scale from that of single scatterers up to the largest features of regional relief.

To remove topographic effects would require that we resolve terrain facets at the 100-m scale of the radar footprint. The accuracy of georeferencing is not good enough for this, and in any case the DEMs available to us, GLOBE and CDED, are both much too smooth for the purpose. As a first step,

we have selected from the series of browse images a set of 20 same-day pairs with reasonable spatial overlap. Most pairs come from days in August and September, but several are from winter months. Each pair consists of an ascending-pass image obtained about ten hours later than a descending- pass image. We examine the change in brightness $\Delta s = s_{asc} - s_{des}$ between the descending-pass and ascending-pass members of each same-day pair in relation to the slope and aspect of the terrain and to the temperature history of the interval between them.

Table 3 summarizes the variation of Δs with slope and aspect. All map cells from all 20 same-day pairs are pooled and averaged for purposes of the summary. To interpret the table, note that the slope and aspect are fixed attributes of the terrain which are viewed by the satellite from different positions. However the azimuths of the sensor do not vary greatly, either within or between images, from means of about 110° and 234° for descending and ascending passes respectively. Thus, for example, terrain elements in the 105°-135° row of the table face towards the sensor on its morning pass, and elements 90° away in aspect are viewed side on (across the slope) by the radar. In the afternoon, terrain in the 225°-255° row faces the sensor.

The estimates of slope and aspect are vector means derived from the DEM. Depending on which DEM is used, we have a sample of either about 20 (GLOBE) or several hundred (CDED) terrain elements per 2x2 km map cell. We do not know which of these elements is actually responsible for backscattering the radar pulse to the sensor. Nor do we know how accurately the actual geometry of each element is represented by the DEM, except that steep slopes are under-represented because of the smoothness of the DEM. Thus, for the slope in particular, the estimates of terrain geometry in Table 3 are quite generalized.

Even after averaging over 20 same-day image pairs, the variation of Δs in Table 3 is substantial, and it is not random in either slope or aspect. Terrain elements facing northeast appear systematically brighter in the morning than in the afternoon (or, equivalently, brighter from southeast than from southwest; we cannot determine whether the effect is due to viewing geometry or to time of day). Elements which face from southeast clockwise to north appear brighter in the afternoon, although the effect is not so pronounced as for the northeast-facing elements. This azimuthal variation is illustrated in Figure 6a.

Brightness difference also varies with gradient, but the average variation (in the bottom row of the table) is less than the average azimuthal variation (in the rightmost column) because the dependence on gradient itself varies with aspect. As illustrated by Figure 7a, there is a cancelling reversal of tendency between terrain elements which face the sensor on descending as opposed to ascending passes. Among elements which face the sensor in the morning (downward triangles in the figure), those which are steeper are brighter in the afternoon. Among elements which face the sensor in the afternoon (upward triangles), those which are steeper are much darker in the afternoon. Moreover, the steepest slopes exhibit a quite distinctive variation with azimuth. In the rightmost column but one of the table, for example, pronounced spikes of opposite sign are evident in Δs for directions facing the sensor on descending (105°-135°) and ascending (225°-255°) passes. It is not known whether these spikes are sampling artefacts; the samples in this column are relatively small.

The features described above recur in many of the single same-day pairs. Figures 6b and 7b are representative examples of brightness differences from a single day. The amplitudes of variation with aspect and slope are greater than in the grand means, but the broad pattern is similar. This day, 10 October 1998, is one on which diurnal meteorological effects are unlikely to have been significant. The Sun was below the horizon, temperature at Colour Lake was below freezing at both overpass times and in the interval between them, and there is unlikely to have been any melting.

Figures 6c and 7c, for 31 July 1999, illustrate a different situation. The variation of Δs with slope is basically similar to that seen earlier, but the azimuthal variation is only weakly developed. The most significant feature in Figure 6c is that the glacierized cells are much darker in the afternoon than in the morning. It may also be significant that the brightness difference for flat terrain is even greater (negatively) than for inclined terrain. In Figures 6a,b and 7a,b the flat-terrain difference was comparable to the average difference for inclined terrain. Evidently something has happened between the times of the two images that cannot be explained in purely geometric-topographic terms.

Figure 8a is a map of Δs for 10 October 1998. Although it is difficult to check at this low spatial resolution, comparison with topographic maps confirms that much and probably most of the variation

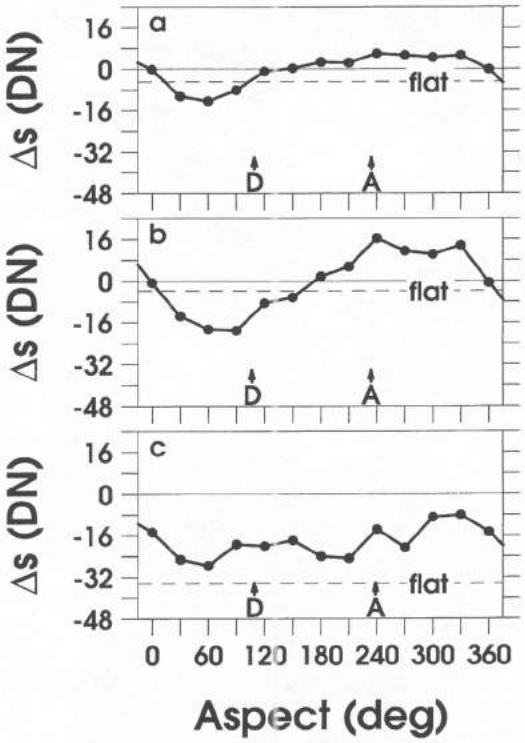

Figure 6. Brightness differences between ascending-pass and descending-pass images from the same day, plotted as a function of the aspect of each map cell. Descending-pass images have local apparent times (LAT) near 0700h. Ascending-pass images have LAT near 1700h. Arrows D,A: mean sensor azimuths. Dashed line ("flat") is average brightness difference for cells with gradients <1°. a: Grand means of differences from 20 same-day pairs in 1998 and 1999 (Table 3). b: Differences for image pair of 10 October 1998 (see also Figure 8a). c: Differences for image pair of 31 July 1999 (see also Figure 8b).

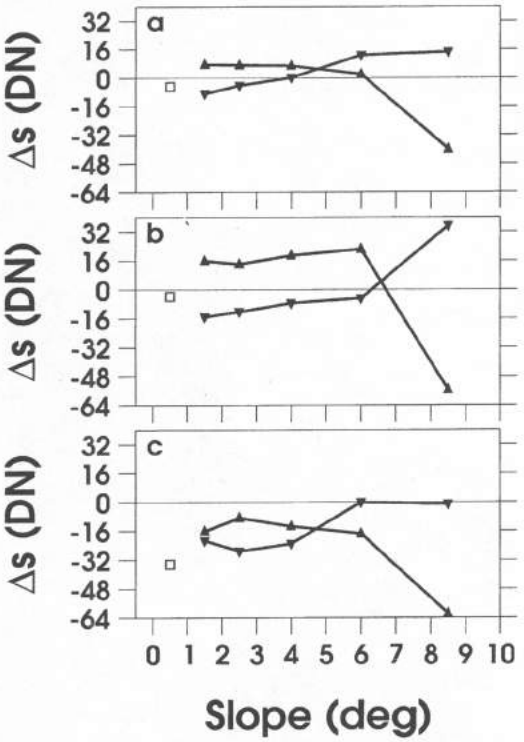

Figure 7. Brightness differences between ascending-pass and descending-pass images from the same day, plotted as a function of the slope of each map cell. a: Grand means of differences from 20 same-day pairs in 1998 and 1999 (see also Table 3). Open square: brightness difference for map cells with slope less than 1°. Downward triangles: differences for cells with aspect between 105° and 135°. Upward triangles: differences for cells with aspect between 225° and 255°. b: Differences for image pair of 10 October 1998, with symbolism as in a (see also Figure 8a). c: Differences for image pair of 31 July 1999, with symbolism as in a (see also Figure 8b).

in Δs is topographically controlled. East- and northeast-facing slopes are darker in the afternoon while west-facing slopes, for example, are brighter in the afternoon. Notice, in the Steacie Ice Cap area of southern Axel Heiberg Island, the roughly north-south orientation of bands of positive and negative brightness difference. The negative bands mark the eastern, and positive bands the western, sides of the ridges which run north-south across the area. Between the ridges are expanded-foot and piedmont glaciers at low elevation, which for the most part exhibit little difference between descending- and ascending-pass brightness. In central Axel Heiberg Island, the higher elevations of Müller Ice Cap also exhibit little difference, while its topographically irregular western parts appear irregular in the figure and its eastern margins, sloping to the east and northeast, show moderately negative differences.

While one can recognize echoes of the topographically controlled patterns of Figure 8a in Figure 8b, for 31 July 1999, the most noticeable feature of this map is the extensive dark portion of the eastern Müller Ice Cap. The dark tone in this difference map corresponds to a darkening of the radar image between morning and afternoon by more than 56 8-bit digital numbers. There are smaller dark patches elsewhere to the south, and the map as a whole is darker than Figure 8a. The darkening of Müller Ice Cap is less towards its eastern margin, and the simplest interpretation of this map is that it records an episode of warming of the firn of the accumulation zone, from a dry and therefore bright

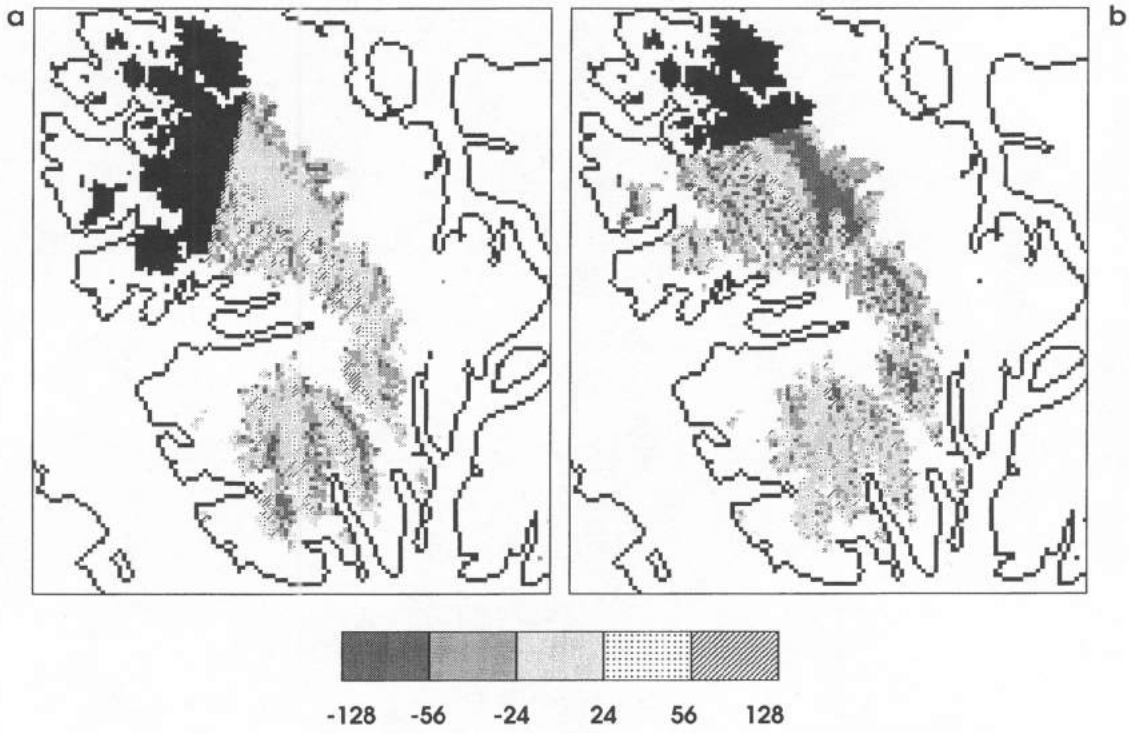

Figure 8. Central and southern Axel Heiberg Island, showing brightness differences between same-day image pairs. Black shading denotes glacierized terrain not appearing in one or both images of the pair. a: 10 October 1998 (see also Figures 6b,7b). b: 31 July 1999 (see also Figures 6c,7c).

state in the morning to a wet and therefore much darker state in the afternoon. The less dramatic darkening to the east occurs over exposed glacier ice. This is also a natural explanation of the contrast between Figure 6b and Figure 6c: in Figure 6c, the advance of melting between morning and afternoon overwhelms whatever purely geometric signal would have resulted from the change in viewing geometry, while in Figure 6b the stamp of the geometric terrain effects is uninfluenced by hydrological changes.

The moderately complex patterns of variation in Table 3 and Figures 6 and 7 are of no glaciological or hydrological interest. We wish to understand them in order to remove them, so as to be better able to concentrate on effects such as those seen in Figure 8b. But the DEM allows us to separate flat terrain from inclined terrain, and therefore to study the interaction between glacier and radar with a significant source of irrelevant variation suppressed. When we screen out all map cells with gradients exceeding 1°, we are still left with a substantial sample of glacierized cells. About 16% of the cells in Table 3 are "flat" in this sense.

Non-geometrical causes of differences between afternoon and morning microwave brightness are most likely to be meteorological. At a latitude of 80°, the solar elevation angle varies little during the day and is in any case symmetrical about solar noon. For the same-day pairs studied here, the afternoon-morning difference in solar elevation angle lies between -0.9° and +2.2°. The Sun was below the horizon on three of the days, including 10 October 1998. Morning temperatures at Colour Lake ranged from -23.6°C to +10.3°C, and the afternoon temperatures were from 0.5K to 6.4K warmer. No particular pattern emerges when Δs is compared to these variables, which is not entirely unexpected. However, if our understanding of the brightness differences is correct, we should expect energy transfer to the glacier to lead to decreases in brightness. The accumulated positive degree-days (PDD) between morning and afternoon images are a useful measure of such energy transfer. PDD models, in fact, are widely used to estimate ablation (e.g., Braithwaite and Zhang 2000).

Figure 9 summarizes an analysis of same-day brightness differences for flat terrain. Average differences for each of the same-day pairs are plotted against PDD. When PDD is zero, Δs is on

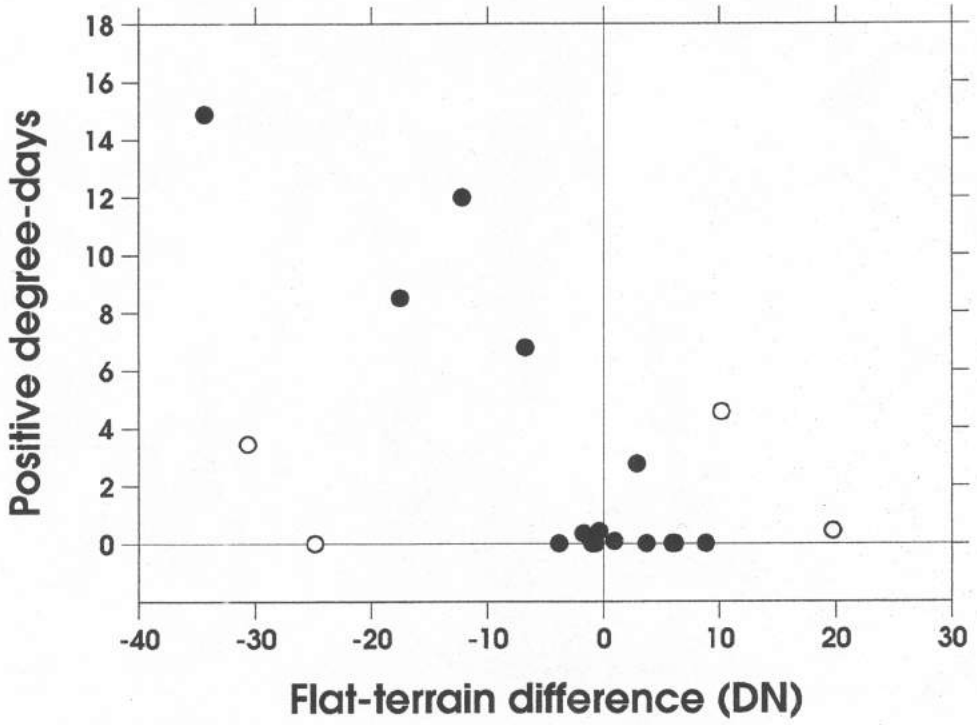

Figure 9. Positive degree-days accumulated in the ~10 hours between early-morning and afternoon members of 20 same-day Radarsat image pairs, as recorded at Colour Lake. Degree-days are plotted as a function of radar brightness differences (afternoon minus early-morning) measured for map cells with gradients less than 1°. Open circles represent possible outliers, as discussed in text.

average positive by a few digital numbers. As PDD increases, Δs grows steadily more negative, indicating that melting during the day has made the radar image darker. The melting observed on 31 July 1999 (Figure 8b) appears as the uppermost symbol in Figure 9.

Although it is encouraging, the alignment of symbols in Figure 9 is far from close. Four of the same-day pairs, identified with a different symbol, stand out as possible outliers. Two have negligible PDD. Two have moderate PDD; both are August pairs, so it is probable that the energy represented by PDD was being transferred to a ripe snowpack and therefore should have produced a darkening. It is difficult to think of glaciological reasons for such changes, and we have excluded most geometric effects by sample selection. One possible geometric effect not accounted for is random variation in the angle of incidence. This arises because the target pixels vary randomly in range (distance from the sensor) from image to image. Axel Heiberg Island is sometimes on the near and sometimes on the far edge of the image, implying a potential variation in i_H from 20° to 50°. With one exception, the afternoon-morning differences in i_H lie between -9° and +6°, so the effect is unlikely to be large. The exception is the image pair for 29 May 1998, for which the average i_H is 41.7° in the morning and 25.5° in the afternoon, a difference of +16.2°. This pair yields the rightmost symbol in Figure 9, but the other three possible outliers are not exceptional in this respect.

As for meteorological (but non-thermal) or operational explanations for the outliers, our temperature record may be intermittently unrepresentative of regional temperature changes, or there may be meteorological changes uncorrelated with Colour Lake temperature, perhaps in precipitation or in the tropospheric humidity profile. It is doubtful, however, that either of these would affect microwave radiative transfer at the Radarsat wavelength. There is nothing in the appearance of the images forming the outlier pairs which would suggest sensor or satellite defects. Gain settings may have been altered between the times of the outlier images. We have no information on this or any other operational possibility, which is a practical limitation of working with browse images.

CONCLUSION

1. Radarsat browse images, as they stand, are shown to be rich and financially attractive sources of information. Their value could be increased markedly by a moderate increase in the amount of accompanying metadata.

2. The radar brightness maps contain information on terrain attributes which, as far as the attempt to identify a signal of melting is concerned, is largely noise. The approach taken here has been to average heavily in the hope of suppressing unwanted random variability. This approach leaves much room for improvement, but it has registered some successes and has confirmed that terrain effects constitute a major bias. It will therefore be essential to model the terrain-related changes with care if routine estimates of the rates of glacier-hydrological processes are to be produced.

3. Although springtime melting of snow cover is observable, it does not appear possible to obtain useful information about ablation by observing exposed glacier ice with radar. Recent studies of microwave imagery (e.g. Engeset and Weydahl 1998; Demuth and Pietroniro 1999; Hall et al. 2000), have shown continued interest in searching for the equilibrium line. Our investigation demonstrates that the information in SAR imagery which is relevant to mass balance is indeed confined to higher elevations on the glacier surface, but it suggests that we need not confine our attention to the annual equilibrium line. In particular, the duration of melting is now a measurable quantity (Cogley 2001), and active-microwave imagery contains extractable information on the intensity of melting.

4. There is a definite proportionality of brightness to temperature in the accumulation zone. At temperatures above freezing, the hotter it is the darker does the appearance of the glacier become. More suggestively, the glacier appears darker as energy transfer to it grows greater. This is a persuasive indication that radar monitoring can become the basis for estimates of glacier melting rates.

5. Substantial effort will be required to realize this promise. The main issues to be resolved may be summarized as: accurate removal of topographic and other non-hydrological noise; better calibration of the radiometric response of wet snow to radar illumination; improvement in understanding of the hydrology of wet snow and firn, at scales from that of snow grains to that of the browse-image pixel; and poor resolution of the ablation zone, requiring investigation of methods for downward extrapolation and validation of information from the accumulation zone. Last but not least, there is no hint as yet of a means of observing accumulation rates remotely.

Acknowledgements

We are grateful to Mike Adair, Canada Centre for Remote Sensing, Natural Resources Canada, Ottawa for information about browse-image processing. Canadian Digital Elevation Data were obtained from Natural Resources Canada through the CRYSYS programme.

REFERENCES

Abdalati, W., and K. Steffen, 1997, Snowmelt on the Greenland Ice Sheet as derived from passive microwave satellite data, *Journal of Climate*, **10**, 165-175.

Adams, W.P., J.G. Cogley, M.A. Ecclestone and M.N. Demuth, 1998, A small glacier as an index of regional mass balance: Baby Glacier, Axel Heiberg Island, 1959-1992, *Geografiska Annaler*, **80A**, 37-50.

Bernier, M., J.-P. Fortin, Y. Gauthier, R. Gauthier, R. Roy and P. Vincent, 1999, Determination of snow water equivalent using RADARSAT SAR data in eastern Canada, *Hydrological Processes*, **13**, 3041-3051.

Braithwaite, R.J., 1984, Can the mass balance of a glacier be estimated from its equilibrium-line altitude?, *Journal of Glaciology*, **30**, 364-368.

Braithwaite, R.J., and Y. Zhang, 2000, Sensitivity of mass balance of five Swiss glaciers to temperature changes assessed by tuning a degree-day model, *Journal of Glaciology*, **46**, 7-14.

Centre for Topographic Information, 2000, Canadian Digital Elevation Data Standards and Specifications. Customer Support Group, Centre for Topographic Information, Natural Resources Canada, Sherbrooke, Quebec. 13p. URL: http://www.ccg.rncan.gc.ca/ext/html/english/products/cded/cded.html.

Cogley, J.G., 2001, Melting on Axel Heiberg Island ice caps from Radarsat browse images, *Annals of Glaciology*, **34**, submitted.

Cogley, J.G., M.A. Ecclestone and W.P. Adams, 1996a, Fluctuations of the terminuses of White and Thompson Glaciers, Axel Heiberg Island, *Eastern Snow Conference Proceedings*, **53**, 83-94.

Cogley, J.G., W.P. Adams, M.A. Ecclestone, F. Jung-Rothenhäusler and C.S.L. Ommanney, 1996b, Mass balance of White Glacier, Axel Heiberg Island, N.W.T., Canada, 1960-91, *Journal of Glaciology*, **42**, 548-563.

Curlander, J.C., and R.N. McDonough, 1991, *Synthetic Aperture Radar, Systems and Signal Processing*. Wiley, New York.

Demuth, M.N., and A. Pietroniro, 1999, Inferring glacier mass balance using Radarsat: Results from Peyto Glacier, Canada, *Geografiska Annaler*, **81A**(4), 521-540.

Engeset, R.V., and D.J. Weydahl, 1998, Analysis of glaciers and geomorphology on Svalbard using multitemporal ERS-1 SAR images, *IEEE Transactions on Geoscience and Remote Sensing*, **36**(6), 1879-1887.

Fahnestock, M.A., R.A. Bindschadler, R. Kwok and K.C. Jezek, 1993, Greenland Ice Sheet surface properties and ice dynamics from ERS-1 SAR imagery, *Science*, **262**(5139), 1530-1534.

Haeberli, W., M. Hoelzle and R. Frauenfelder, 1999, *Glacier Mass Balance Bulletin No. 5 (1996-1997)*. International Commission on Snow and Ice of International Association of Hydrological Sciences/UNESCO, Paris.

Hall, D.K., R.S. Williams Jr., J.S. Barton, O. Sigurðsson, L.C. Smith and J.B. Garvin, 2000, Evaluation of remote-sensing techniques to measure decadal-scale changes of Hofsjökull ice cap, Iceland, *Journal of Glaciology*, **46**(154), 375-388.

Hastings, D.A., and 13 others, eds., 1999, The Global Land One-kilometer Base Elevation (GLOBE) Digital Elevation Model, Version 1.0. National Oceanic and Atmospheric Administration, National Geophysical Data Center, 325 Broadway, Boulder, Colorado 80303, U.S.A. Digital data base on the World Wide Web (URL: http://www.ngdc.noaa.gov/seg/topo/ globe.shtml) and CD-ROMs.

Olmsted, C., 1993, *Alaska SAR Facility Scientific SAR User's Guide*. ASF-SD-003. Alaska SAR Facility, Fairbanks, Alaska. 57 p.

Ommanney, C.S.L., 1969, *Glacier Inventory of Canada - Axel Heiberg Island, Northwest Territories*. Technical Bulletin 37, Inland Waters Branch, Department of Energy, Mines and Resources, Ottawa. 97p.

Østrem, G., 1975, ERTS data in glaciology - an effort to monitor glacier mass balance from satellite imagery, *Journal of Glaciology*, **15**, 403-414.

Paterson, W.S.B., 1994, *The Physics of Glaciers*. 3rd edition. Pergamon, Tarrytown, New York. 480p.

Raney, R.K., 1998, Radar fundamentals: technical perspective, in Henderson, F.M., and A.J. Lewis, eds., *Principles and Applications of Imaging Radar (Manual of Remote Sensing, Third edition, Volume 2)*, 9-130. Wiley, New York. 866p.

Seeber, G., 1993, *Satellite Geodesy*. de Gruyter, Berlin, 531p.

Smith, L.C., R.R. Forster, B.L. Isacks and D.K. Hall, 1997, Seasonal climatic forcing of alpine glaciers revealed with orbital synthetic aperture radar, *Journal of Glaciology*, **43**(145), 480-488.

Stiles, W.H., and F.T. Ulaby, 1980, The active and passive microwave response to snow parameters 1. Wetness, *Journal of Geophysical Research*, **85**(C2), 1037-1044.

U.S. Army Corps of Engineers, 1956, *Snow Hydrology*. North Pacific Division, Corps of Engineers, U.S. Army, Portland, Oregon. 437p.

Zwally, H.J., and S. Fiegles, 1994, Extent and duration of Antarctic surface melting, *Journal of Glaciology*, **40**(136), 463-476.